Approaching the numerical aperture of water - Immersion lithography at 193nm

Bruce W. Smith, Anatoly Bourov, Yongfa Fan, Lena Zavyalova, Neal Lafferty, Frank Cropanese,
Rochester Institute of Technology, Microelectronic Engineering Department
82 Lomb Memorial Drive, Rochester, NY 14623-5604

ABSTRACT

As immersion nanolithography gains acceptance for next generation device applications, experimental data becomes increasingly important. The behavior of resist materials, fluids, coatings, sources, and optical components in the presence of a water immersion media presents conditions unique compared to convention "dry" lithography. Several groups have initiated fundamental studies into the imaging, fluids, contamination, and integration issues involved with water immersion lithography at 193nm. This paper will present the status and results of the next stage of the development efforts carried out at RIT. The status of two systems are presented; a small field projection microstepper utilizing a 1.05 catadioptric immersion objective lens and a 0.50 to 1.26NA interferometric immersion exposure system based on a compact Talbot prism lens design. Results of the fundamental resolution limits of resist materials and of imaging optics are presented. Additionally, an exploration into the benefits of increasing the refractive index of water is addressed through the use of sulfate and phosphate additives. The potential of KrF, 248nm immersion lithography is also presented with experimental resist imaging results.

Keywords: immersion lithography, high NA, 193nm

1. INTRODUCTION

Though immersion microscopy has been utilized for high resolution imaging for over 100 years [1], its extension to immersion lithography had not been considered commercially practical until very recently. Water was proposed as a viable immersion fluid by Smith and Kang in 2000 and immersion lithography was demonstrated initially at a k_1=0.27 for 100nm features at 1.2 NA using the 442nm wavelength of a HeCd laser [2]. Recent developments at 193nm, combined with continual challenges faced with 157nm and EUV technology, has positioned water immersion lithography as the next generation technology to extend optical lithography to sub-45nm device generations.

A study of the feasibility of water immersion lithography at 193nm was reported earlier [3]. In that report, we describe the potential resolution and focal depth improvements enabled with the technology as well as some key enabling challenges. Since then, studies have been conducted in areas of fundamental resolution limits, polarization and high NA effects, immersion fluids properties, and microbubble effects. This follow-up paper addresses these aspects of water immersion lithography.

2. THE OPTICAL POTENTIAL OF IMMERSION LITHOGRAPHY

Interferometric lithography provides an opportunity to explore lithographic imaging at oblique propagation angles and extreme NA imaging. Through interferometric imaging, a sinusoidal standing wave pattern is created through the interference of coherent wavefronts. Through the control of the number of wavefronts and their corresponding interference angle, the orientation, pitch and dimensionality of geometry can be controlled. By including a non-interfering component, imaging can be tailored to synthesize various conventional projection imaging situations. Through variation of the phase character of a plurality of wavefronts, imaging can be matched to those obtained using partially coherent projection lithography. The advantage of using interferometric lithgraphy as a method to achieve such images is the versatility to allow for high NA values and immersion imaging media.

The application of a Talbot interferometer has been used for excimer laser interferometric imaging [4]. The approach that we have taken is a variation of such a system where first order beams are split using a phase grating and recombined

using a pair of mirrors to for an interference pattern. The setup is shown in Figure 1. In a system with d/2 reduction (where d is the grating pitch on the phase mask), the approach leads to an achromatic system when angles at the grating and image planes are equivalent. This is a consequence of the preservation of path length and spatial coherence within the beams. In this system, a grating pitch of 600nm is used, resulting in a numerical aperture (NA) on the mask side of 0.16. An increase in NA at the image plane is achieved through angular control of reflecting surfaces.

Figure 2 show results obtained using water immersion interferometric lithography. Images are sequenced according to line size where each case was produces at numerical aperture values according to $0.5\lambda/p$, where p is the full cycles pitch of the patterns. Resolution from 80nm to 38nm has been demonstrated using immersion numerical aperture values between 0.5 and 1.26 and TE polarized illumination. A Shipley XP-1020 resist was used for each case, coated over an AR layer with a TOK TSP-03 top coat. Resist film thickness ranged between 50 and 100nm. Of particular interest are the 38nm features, which are 1:1 duty ration in 50 and 70nm resist films. The image modulation is remains high, despite moderate resist failure at these dimensions.

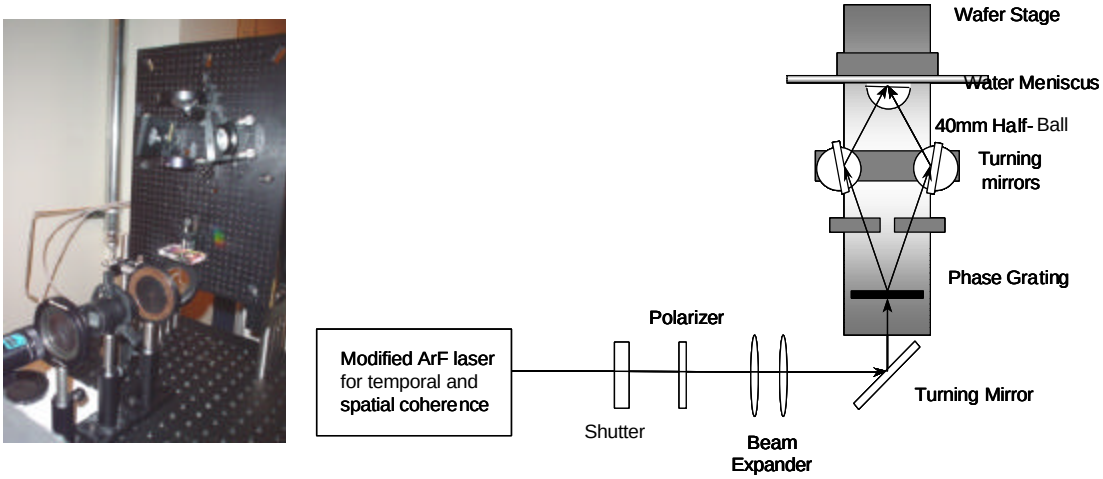

Figure 1. Set-up and schematic diagram of the 193nm Talbot interferometric immersion lithography system.

A compact alternative to the Talbot interferometer is shown in the prism lens shown in Figure 3, which is also described in a paper by Bourov et al [5]. The lens is based on a fused silica prism with surfaces polished and coated to produce a magnification in the numerical aperture of a phase grating. For example, a 600nm pitch phase gating placed at the low-NA side of a prism with 160 degree reflective faces. First diffraction orders from the phase grating are directed toward the image plane at a numerical aperture in fused silica of 0.83. A 1 mm meniscus of water is held between the image plane and the prism, resulting in an effective immersion numerical aperture of 1.2 or a resist image pitch of 80nm. The availability of several prisms allows for a range of numerical apertures or pitch values. Since the prisms can be fabricated with X and Y polished surfaces, imaging of horizontal and vertical lines are possible as well as contact hole features using four (or five) beams. Any residual zero order resulting from the phase grating can be eliminated by blocking its path through the interferometer. Figure 5 shows image results from a 1.05NA compact Talbot prism lens operating at a NA of 1.05. Features are 45nm (1:1) imaged in 70nm resist thickness. Other feature resolution is obtained with lenses described in Table 1.

193 Prism Lens Designs

NA	***half-pitch***
0.8	***60nm***
1.05	***45nm***
1.20	***40nm***
1.35	***36nm***

Table 1. Prism lens numerical aperture values and corresponding half-pitch for compact Talbot lens designs.

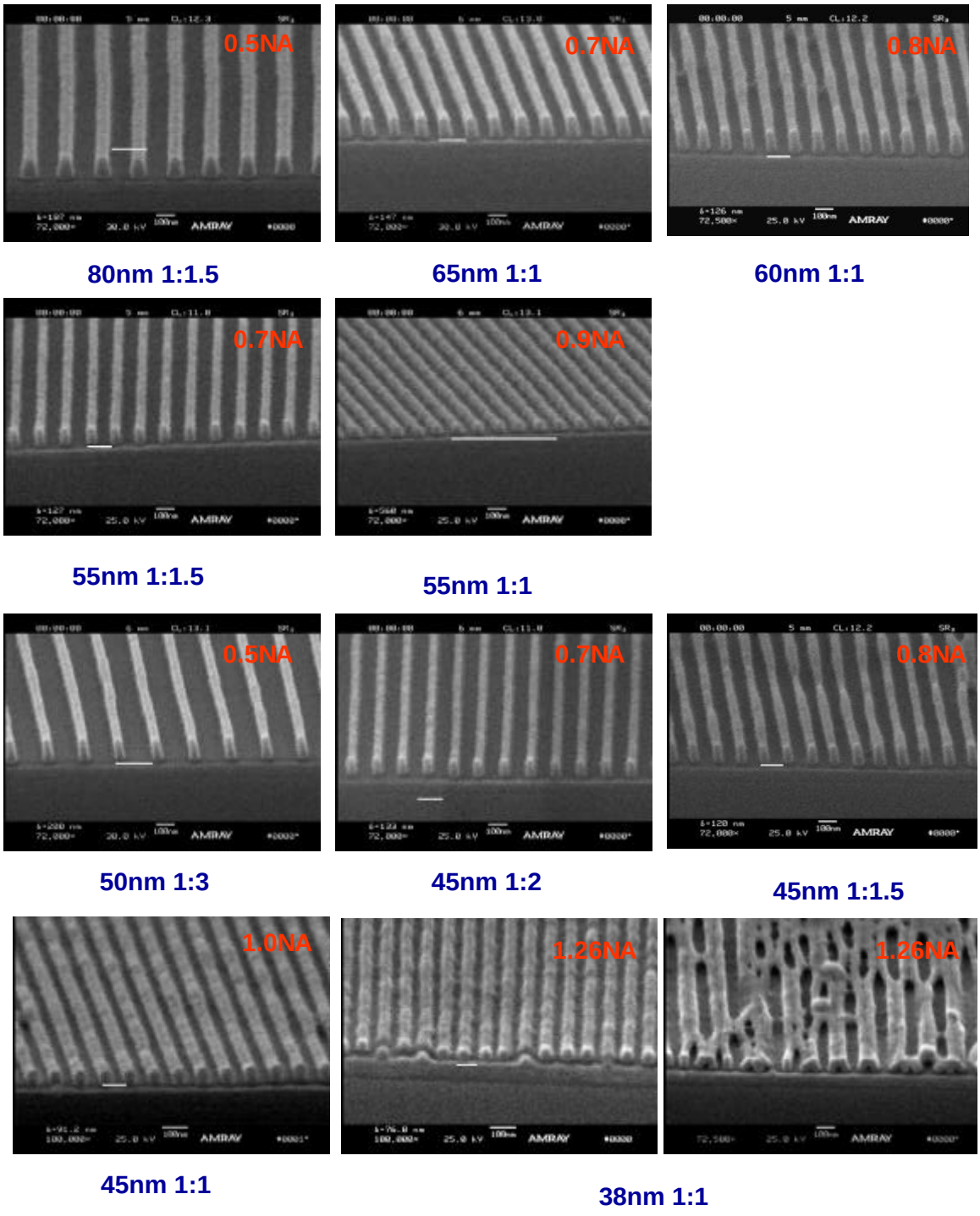

Figure 2. Resist images at 193nm using water immersion lithography for feature sizes from 80nm to 38nm. Corresponding NA values range from 0.50 to 1.26.

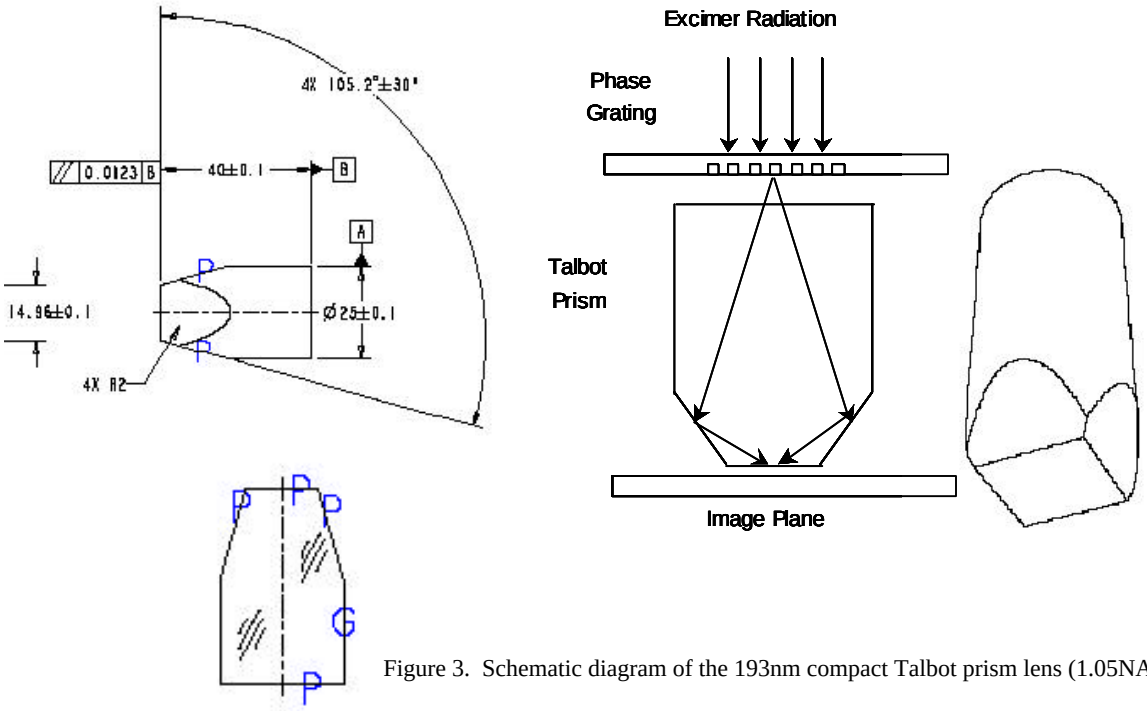

Figure 3. Schematic diagram of the 193nm compact Talbot prism lens (1.05NA).

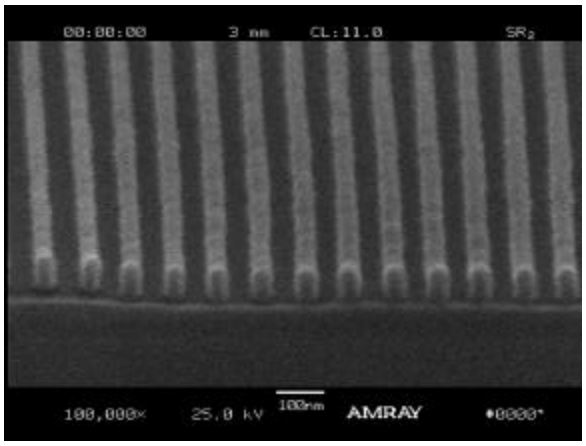

Figure 4. Resist images of 45nm half-pitch from 1.05NA compact prism lens.

3. IMMERSION PROJECTION MICROSTEPPER

A small field projection microstepper has been assembled utilizing a catadioptic immersion fused silica projection lens from Corning / Tropel, and an Exitech PS5000 micro-exposure tool. The system is capable of 200mm XY Motion using a hybrid mechanical – air bearing design with accuracy better than ±2µm/100mm travel. Z axis motion is controlled with 3-point piezoelectric Z elevator for sub-5nm positioning resolution. Height sensing resolution and repeatability is better than 25nm. The Corning / Tropel AquaCAT lens allows operating with the following specifications. The optical performance of the lens is also described in a companion paper [6].

Property	*Performance*
NA	1.05
Reduction	90X
Image field	0.1 mm
Wavelength	193.3 nm
Bandwidth	700 pm
Track length	210 mm +/- 10 mm
Working distance	>0.5 mm
Number of elements	8
% Obscuration	<15%
Measured wavefront	<0.05 waves rms

Figure 5 shows a schematic of the system optical train and the tool installation. Figure 6 shows diagram of the AquaCAT lens. Initial imaging results with the system are shown in Figure 7, where 100nm resist resolution has been achieved using a binary mask at a partial coherence factor of 0.7 in a TOK ILP03 resist over a Brewer AR29 BARC and a TOK immersion resist topcoat.

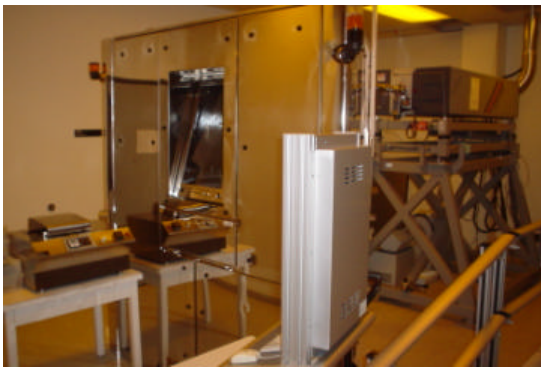

Figure 5. Exitech 193nm immersion projection system.

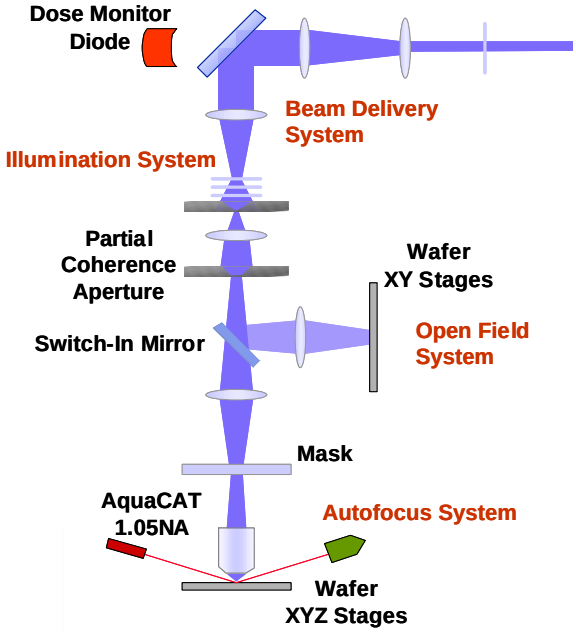

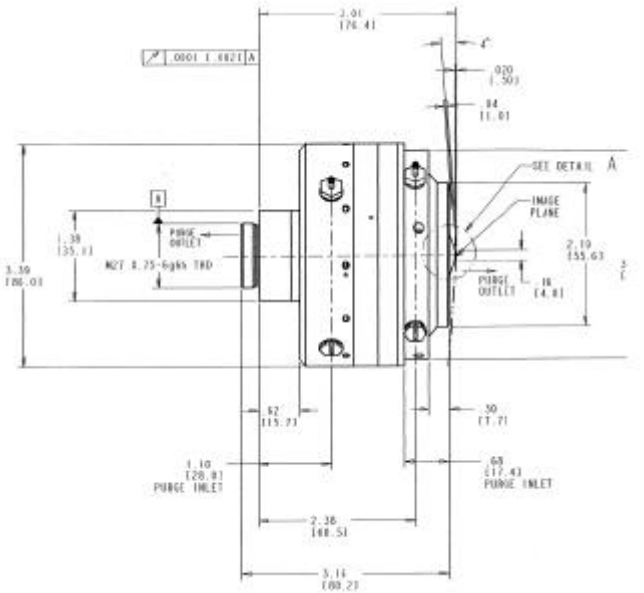

Figure 6. Corning Tropel 1.05NA AquaCAT 193nm immersion projection lens.

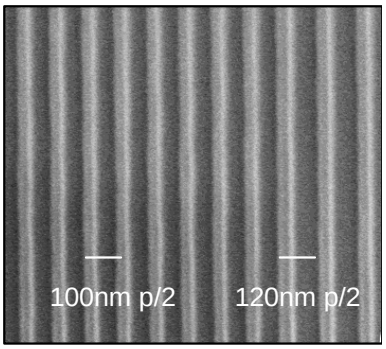

Figure 7. Initial 100 – 120nm resist image results from Exitech system with AquaCAT lens using a binary mask and 0.7 σ.

4. OPTICAL IMPACT OF MICROBUBBLES

In the process of forming a water fluid layer between the resist and lens surfaces, air bubbles are often created due to the high surface tension of water. The presence of air bubbles in the immersion layer will degrade the image quality because of the inhomogeneity induced light scattering in the optical path. Therefore, it is essential to understand the air bubble induced light scattering effect on image quality. We report on details of geometrical optical and Mie scatter analysis in our companion paper [7].

Scattering of air bubbles in water can be approximately described using a geometrical optics model [8]. An air bubble assumes a spherical shape in water when the hydraulic pressure due to gravity is ignored. The assumption is reasonable in lieu of immersion lithography where a thin layer of water with thickness of about 0.5 mm is applied. The reflection/refraction at the spherical interface causes the to light stray into various directions, i.e. scattering. The relevant reflection/transmission coefficients can be approximated by flat surface Fresnel coefficients. However, the air bubble in water is a special case, where the refractive index of the bubble is less than that of the surrounding media, resulting in a contribution of total reflection to scattered irradiance at certain angles. The situation is described in Figure 8. For an arbitrary ray incident on a bubble, the angle of incidence is $i = arcsin(s/a)$, where a is the radius of the bubble, s is the deviation from the center. The critical incident angle is

$$i_c = arcsin(n_i / n_w) \tag{1}$$

where n_i is the refractive index of the air, n_w is the refractive index of water. The corresponding critical scattering angle is:

$$q_c = 180° - 2i_c \tag{2}$$

At a wavelength of 193 nm, the refractive index of water is n_w=1.437. Therefore, the critical incident angle and critical scattering angle are,

$$i_c = arcsin\left(\frac{1}{1.437}\right) = 44°$$
$$q_c = 180° - 2i_c = 92°$$

The presence of total reflection greatly enhances the light scattered into the region subtended by . In this case, the region covers all the forward directions. Hence, air bubbles in water cause strong scattering in all the forward directions. However, a complete understanding of scattering will require taking into account the effects of interference of the reflected light with other transmitted light. The rigorous solution of the scattering pattern can be numerically evaluated by partial wave (Mie) theory.

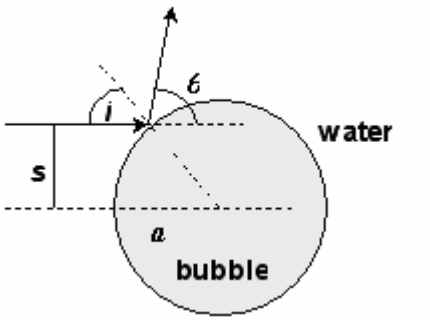

Figure 8. Geometric description of an air microbubble in water.

In Mie scattering theory the incident, scattered, and internal fields are expanded in a series of vector spherical harmonics [9]. The coefficients of these expansion functions are chosen so that the tangential components of the electric and magnetic fields are continuous across the surface of the sphere. Two calculation parameters are needed to specify a scattering case, the relative refractive index $m = n_i / n_w$ and the size parameter $ka = 2p \frac{n_w a}{n_i l_i}$. The scattering irradiance can be calculated from the following:

$$i_j = i_{inc} I_j a^2 / 4R^2 \qquad (3)$$

$$I_j = \left|S_j\right|^2 (2/ka)^2 \qquad (4)$$

where subscript j denotes the polarization orientation (j=1, perpendicular to scattering plane; j=2, parallel to scattering plane). The term i_j is the scattered irradiance, i_{inc} is the incident irradiance, I_j is the normalized scattered irradiance, R is the distance from the bubble to the far-field observation point, and S_j is the complex scattering amplitudes. S_j can be evaluated from the Mie series. At the wavelength of 193 nm, the scattering of an air bubble 2 μm in diameter was calculated according to Mie theory and plotted in Figure 9.

At the wavelength of 193 nm, air bubbles are transparent with a refractive index of approximately 1.0. Ideally, a synthetic sphere with refractive index of 1.874+0i (so that the refractive index difference with water is the same as air bubble) would serve the purpose. Polystyrene (PST) spheres (n=1.67+1.02i) provide close a match to these optical properties. Mie scattering calculations of spheres 2 μm in diameter were conducted with the results plotted in Figure 10. Evaluation of scattering due to air bubbles and PST spheres was conducted for TE, TM or unpolarized incident light. Comparison of the scattering patterns shows that the PST spheres and air bubbles resemble each other with respect to scattering properties. Hence polystyrene spheres are used to mimic air bubbles in studies of lithographic imaging of "bubbles" in immersion water. In direct interference lithography, it is found that PST spheres (2 μm in diameter) 0.3 mm away from the resist surface would not image, while for interferometric lithography at 0.5NA, this distance is estimated to be 1.3 mm. Surprisingly, polystyrene spheres in diameter of 0.5 μm (which is 5 times larger than the interferometric line-width) will not image. It is proposed that "bubbles" are repelled from contact with the resist film by surface tension. The scatter of exposure light can be characterized as "flare" effect. This work shows that microbubbles are not a technical barrier to immersion lithography.

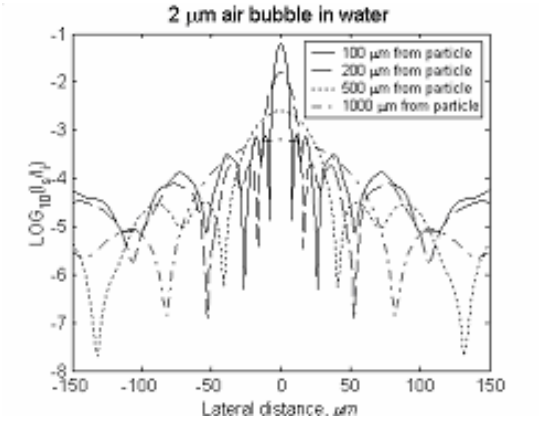

Figure 9. Mie scatter modeled for a 2 μm air bubble in water at various separation distances.

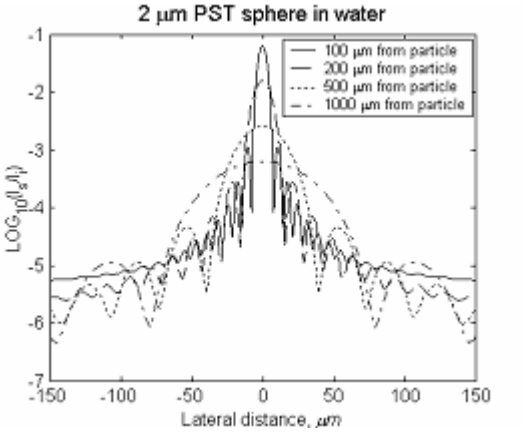

Figure 10. Mie scatter modeled for a 2 μm PST sphere in water at various separation distances.

5. IMMERSION FLUIDS AND WATER ADDITIVES

An imaging system using an immersion fluid is shown in Figure 11. The left portion of this figure depicts an optical wavefront created by a projection imaging system, which is focused into a photoresist (resist) material with refractive index n_r. The refractive index of the imaging media is n_a (and in this example is air). The right portion of the figure depicts an optical wavefront focused through a media of refractive index larger than the one on the left, specifically n_m. As the refractive index nm increases, the effect of defocus, which is proportional to $\sin^2\theta$ is reduced. Furthermore, as shown in Figure 12, a refractive index approaching that of the photoresist is desirable to allow for large angles into the photoresist film and also allow for reduced reflection at interfaces between the media and the resist. Ultimately, a small NA/n is desirable in all media and the maximum NA of the system is limited to the smallest medial refractive index. The goal then becomes matched indices or *homogeneous immersion* (a term coined by Abbe in 1878).

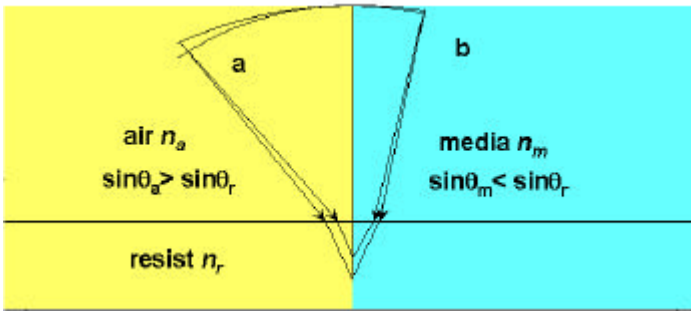

Figure 11. Spherical wavefront showing the effect of air and higher index media on defocus.

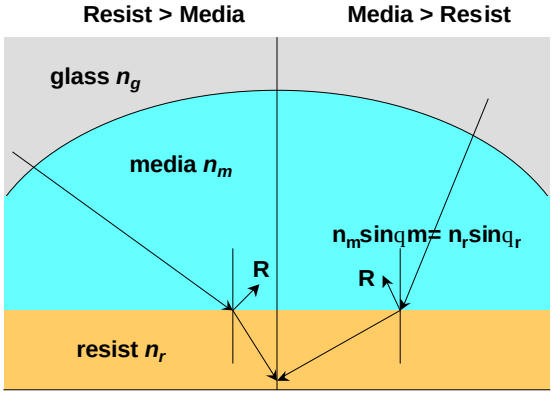

Figure 12. Reflection and refractive effects for high and low refractive index media.

We have initiated studies to increase the refractive index of water from its natural value through the addition of compounds that introduce acceptably low absorption to the water. In general, the UV absorption of a material involves the excitation of an electron from the ground state to an excited state. When solvents are associated, additional "charge-transfer-to-solvent" transitions (CTTS) are provided [10, 11]. The absorption wavelength resulting from CTTS properties and absorption behavior of aqueous solutions of halide ions follow the behavior:

$$F^- < (OH)^- < Cl^- < Br^- < I^-$$

where fluoride ions absorb at shorter wavelengths than iodide. Table 1 shows the effect of several anions on the absorption edge of water [12]. The presence of alkalai metal cations can shift the maximum absorbance wavelength to lower values, following the following behavior:

$$Cs^+ < Rb^+ < K^+ < Li^+ < Na^+ < NH4^+ < H3^+O$$

Furthermore, the change in the absorption with temperature is positive and small (~500ppm/°C), while the change with pressure is negative and small.

The absorption of several families of materials dissolved in water has been measured. These materials include chlorides, iodides, fluorides, bromides, phosphates, and sulfates. Figure 13 and 14 show the absorption properties of sulfates and phosphates. The molar absorbance (absorbance per mm per mol/liter) is given for each material along with the unit absorbance [mm^{-1}] for each particular sample. Samples were measured using a Perkin Elmer UV-visible spectrophotometer, model UV11, and quartz fluid sample holders in the path of the beam. For each sample, a pair of measurements were taken at 1mm and 2mm sample thicknesses for differential calculation of absorbance. Several of these materials show sufficiently low absorbance at wavelengths between 180nm and 300nm.

The refractive index of three examples of water solutions of compounds from Figures 13 and 14 are shown in Figure 15. The three fluids, cesium sulfate, hydrogen sulfate (sulfuric acid) and hydrogen phosphate (phosphoric acid) each show refractive index values above that for pure water, while allowing large transmission through low absorption. All refractive index measurements were taken using spectroscoptic variable angle ellipsometry using a Woollam WVASE tool (WVASE-DUV). For each sample, a film was created on a fused silica samplewhich was made rough by bead blasting the front surface. This allowed a fluid film to adhere to the substrate and allowed for ellipsometric fitting of refractive index using the data generated by the tool.

The refractive index values achieved with the three fluids at 193nm are as follows. Each solution is identified by the concentration (by weight for CsSO4 or by volume for acids), refractive index at 193nm, the maximum numerical aperture allowed (NAmax) at 193nm, and the minimum resolution allowed at 193nm (Rmin).

Fluid	Refractive index	NAmax	Rmin
Water	1.44	1.44	33.7nm
H2SO4 19% by volume	1.48	1.48	32.6nm
Cs2SO4 40% by weight	1.60	1.60	30.2nm
H3PO4 17% by volume	1.63	1.63	29.6nm

Figure 16 shows resist images created using water alone as an imaging media and water with 40 wt% of CsSO4. The figure shows results for a 31 degree angular aperture (propagation angle) in each fluid. The corresponding numerical aperture in water is 0.70 while the corresponding numerical aperture in CsSO4 is 0.78. This demonstrates a 11% improvement in resolution of the imaging using the additive to the water. H2SO4 would provide a 4% improvement and H3PO4 would provide for a 13% improvement.

as

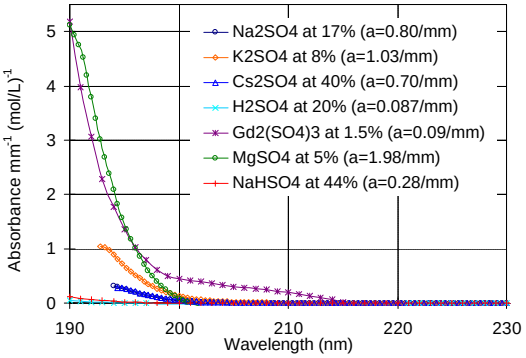

Figure 13. UV absorbance of various sulfates in water.

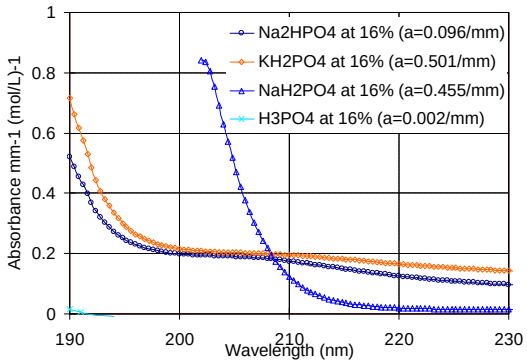

Figure 14. UV absorbance of various phosphates in water.

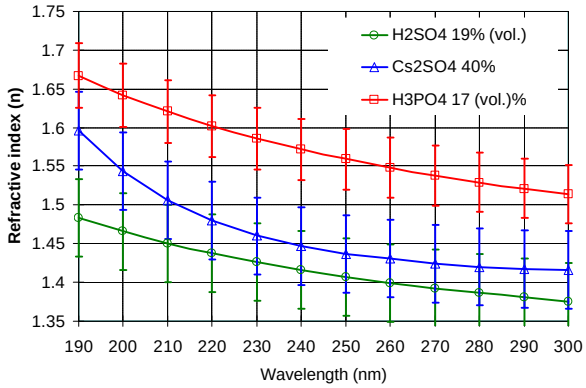

Figure 15. Refractive index of water with sulfate and phosphate additives.

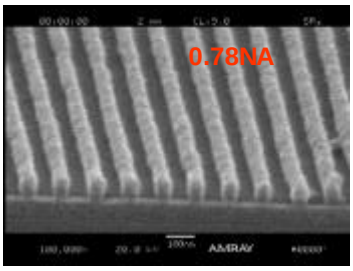

59nm 1:1 (50nm resist)

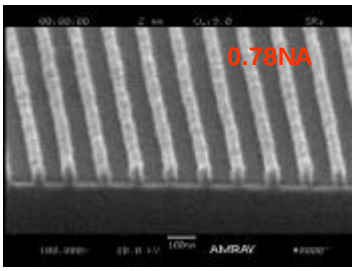

39nm 1:2 (50nm resist)

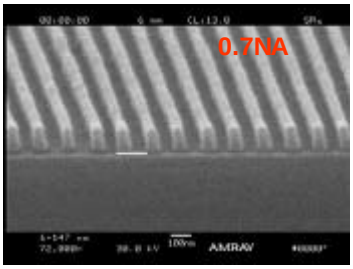

65nm 1:1 (100nm resist)

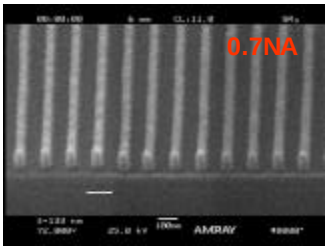

45nm 1:2 (70nm resist)

Figure 16. Comparison of resist images using cesium sulfate solution (top) and water (bottom) immersion fluids. The numerical aperture values of 0.78 (sulfate) and 0.70 (water) are a result of identical angles in the immersion fluids (31°).

6. POLARIZATION AT IMMERSION NA VALUES

Polarization issues become increasingly important as immersion lithography is considered for next generation optical lithography. The critical implications of immersion lithography are not limited to the lens design, materials, contamination, and fluid control issues that are under exploration as extreme propagation angles are enabled by the technology. As radiation propagates through an optical system, it is influenced by reflection, refraction, and interference (and diffraction). As the polarization state of radiation is considered, it is important to consider the components within the system that can be influenced. The impact of polarization in three critical locations is described in a companion paper, namely in the illumination plane, in the mask plane, and in the image plane [13].

7. IMMERSION LITHOGRAPHY AT 248NM

Since the absorption of water at wavelengths above is low, its application as an immersion fluid may be extendable toward 248nm. With further separation from the absorption edge however, the refractive index decreases. Measurements of the refractive index of water indicate that a value near 1.39 can be expected [14]. The Talbot interferometric lithography system described in Section 2 was modified for use with a KrF 248nm excimer fitted with extra-cavity spatial and temporal filtering can allow for a ~1mm temporal coherence length and ~5pm spectral bandwidth. A 600nm phase grating mask was used where residual zero diffraction order was filtered. The immersion system was configured for a numerical aperture of 0.83, corresponding to 75nm half-pitch resolution. A Shipley experimental 248nm resist was coated to 100nm over a compatible ARC layer and a TOK TSP-03 top coat was applied. Initial images are shown in Figure 17.

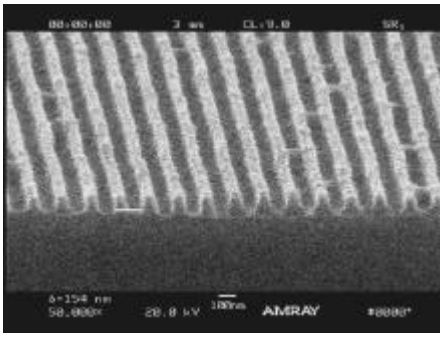

Figure 17. Initial 248nm water immersion lithography results of 75nm half pitch features at 0.82NA.

8. CONCLUSIONS

Significant progress has been made in the area of immersion lithography since it was first proposed as a potential candidate for next generation optical lithography. Images of 38nm half-pitch are close to the theoretical limits of 33.5nm possible with water at 193nm. We have described several areas that have been a concern for the application of this technology with few technical barriers to allow additional progress toward sub-45nm device generations. As progress is made with additives for water to raise its natural refractive index, the potential increases for 193nm lithography to remain a viable alternative for 32nm applications.

9. REFERENCES

[1] E. Abbe, 1878.
[2] B. W. Smith, H. Kang., A. Bourov, P. Rack, “Optical Research for UV and VUV SRC Contract 775,” SRC Program Review 2000 (July 2000).
[3] B. W. Smith, A. Bourov, H. Kang, “Water Immersion Optical Lithography at 193nm,”, JM3, 3(1) (2004) 44.
[4] P.E. Dyer, R.J. Farley, R. Giedl, Opt. Comm, 129, 1996, 98.

[5] A. Bourov, Y. Fan, Frank C. Cropanese, N. Lafferty, L. Zavyalova, B. W. Smith, “Immersion microlithography at 193 nm with a Talbot prism interferometer,” Proc. SPIE 5377 (2004).
[6] P. Dewa et al, “Optical Metrology for 193-nm Immersion Objective Characterization,” Proc. SPIE 5377 (2004).
[7] Y. Fan, N. Lafferty, A. Bourov, L. Zavyalova, B.W. Smith, “Study of air bubble induced light scattering effect on image quality in 193-nm immersion lithography,” Proc. SPIE 5377 (2004).
[8] P. L. Marston, “Light scattering from bubbles in water”, Ocean 89 Part 4, Acoust. Arct. Stud., pp. 1186-1193, 1989.
[9] C. F. Bohren, D. R. Huffman, Absorption and Scattering of Light by Small Particles, John Wiley & Sons, 1983.
[10] E. Rabinowitch, Rev. Mod. Phys., 14, 112 (1942).
[11] G. Stein and A. Treinen, Trans. Faraday Soc. 56, 1393 (1960).
[12] M.J. Blandamer and M.F. Fox, Theory and Applications of Charge-Transfer-To-Solvent Spectra, (1968).
[13] B. W. Smith, L. Zavyalova, A. Estroff, “Benefiting from Polarization – Effects on High-NA Imaging,” Proc. SPIE 5377 (2004).
[14] P. Schiebener, J. Straub, J.M.H. Levelt Sengers and J.S. Gallagher, J. Phys. Chem.Ref. Data 19, 677, (1990).